ARTICLES

Density Functional Theory Study of Copper Clusters

Perla B. Balbuena,*,† Pedro A. Derosa,† and Jorge M. Seminario*,‡

Department of Chemical Engineering, Swearingen Engineering Center, and Department of Chemistry and Biochemistry, University of South Carolina, Columbia, South Carolina 29208

Received: June 25, 1998; In Final Form: February 9, 1999

A density functional theory study of copper clusters is presented. Fully optimized geometries, electronic structures, HOMO−LUMO gaps, spin density distributions, and ionization potentials are reported. The study is systematic starting with one-dimensional clusters followed by several planar structures and three-dimensional systems chosen to emulate (100) and (111) planes of bulk Cu. For the 1-D systems, it is found that the dissociation energy and ionization potential follow an oscillatory behavior that reflects a conjugate-like character indicative of a pair-occupation nature of copper. Calculated bond lengths, vibrational modes, ionization potentials, and dissociation energies for the smallest clusters agree very well with the available experimental information. A 1-D limit is rapidly reached by a chain system of 15 atoms. Most of the analyzed properties show substantial differences between the end atoms and those occupying central locations. The chain central atoms, with largest coordination numbers, bear the highest negative charge in the linear chains, and the same feature is observed in planar and 3-D structures. A semiempirical expression dependent on the cluster average coordination number is used to investigate the connection between the calculated cluster ionization potential and the local work function. The study confirms the validity of the cluster approach to improve the understanding of physicochemical properties at interfaces.

1. Introduction

With the tremendous advances in the development of new experimental techniques for the microscopic understanding of the physics and chemistry of surfaces, a great deal of experimental and theoretical work has been oriented to the investigation of small particles, microcrystals, and clusters.[1] One of the most important surface properties is the work function (WF), which is by definition the amount of energy needed to extract one electron from a given surface. This property plays an important role in the design of several technological applications, which explains why a large number of theoretical and experimental efforts have been directed to its characterization. For example, the existence of quantized levels in thin metal films was determined from a calculation of the WF.[2] Correlations between WF and surface energy have permitted characterization of electrochemical adsorption processes based on measurements of WF changes.[3−5] Open circuit voltage in batteries has been related to the difference of cathode and anode WFs.[6] Due to the strong dependence of the WF on the surface structure, measurements of metal WFs yield information about the microscopic structure of the surface, allowing the characterization of crystallographic orientations and other detailed structural and chemical information of virgin and modified surfaces.[7]

Measurements of metal WF are based on metal ionization by application of an external electrical field, heating, or absorbing a photon on the surface.[8] In all cases, an average work function is obtained because the experiment reflects an average of all surface heterogeneities existing at the atomistic level. The concept of local work function has triggered new experiments such as photoemission of adsorbed xenon that are able to detect local variations of work function on bimetallic or defective surfaces.[7]

Previous approaches based on phenomenological Hamiltonians[9−14] have determined the WF as the difference of the Fermi level of a bulk crystal, minus the height of a barrier due to interactions with surface image charges that a leaving electron needs to overcome. Other methods have successfully determined the WF from calculations on large clusters but imposing restrictions on some degrees of freedom of the system.[15] Although the WF can be calculated exactly solving the Schrödinger equation for the neutral and corresponding ionized system using the real Hamiltonian, the problem is very demanding computationally. On the other hand, the ionization potential (IP) of small clusters can be calculated with chemical accuracy. Such cluster systems retain the main characteristics responsible for local variations of the bulk work function. The IP of a finite cluster differs from the bulk WF, since the latter is actually an average of several nonequivalent points, and the former is as exact as the electronic description used, although corresponding to a finite system.

To understand from first principles macroscopic properties, it is important to determine how the IP and other related cluster properties evolve to bulk values. In addition, some applications rely on differences of WF rather than in their absolute values, such as the changes in WF associated with atom intercalation, vacancies, or defects. In these situations, the relative values do not reflect the cluster−bulk differences due to intrinsic error

* Corresponding authors. Fax: (803)-777-8265. E-mail: Perla@sun.che.sc.edu.
† Department of Chemical Engineering.
‡ Department of Chemistry and Biochemistry.

10.1021/jp982775o CCC: $18.00
Published on Web 03/26/1999

cancellations. Moreover, the cluster approach presents the advantage that one can build a surface with the desired characteristics and determine its IP provided the electron leaves the system through the surface of interest, which is easily determined from the location of the highest occupied molecular orbital. Precise first principles calculations on well-characterized clusters have proven to be useful in providing details on electronic interactions that complement and guide experimental studies.[15−18] These studies are relevant because small clusters are, in many cases, the active components of dispersed metal catalysis, due in part to their large surface-to-volume ratio. Other applications of metal clusters involve the nucleation and growth of metal microclusters used as basic materials in photographic processes. In addition, the special features of small metal clusters, such as metal−insulator transitions, can be used in the design of novel sensors.[19] The advent of molecular electronics where single molecules are assembled "one by one" [20−22] demands also precise studies of small clusters.[23] In all of these processes, the cluster, rather than the bulk properties, are needed for the proper characterization of the systems. Most importantly, cluster representations are fundamental in order to evaluate chemistry on surfaces.

In this work we use DFT to investigate the electronic structure of several fully optimized copper clusters. We study the relationship between selected cluster properties as functions of the number of atoms and of the system dimensionality. As in many practical situations, we start with a one-dimensional model, because with the current computational resources it is very likely that this is the only case where one can observe the cluster-to-bulk evolution of properties. This approach is similar to the one used in quantum mechanics where the one-dimensional box is used as the starting point for further studies of more realistic systems. As discussed by Hoffmann,[24] much of the physics of two- and three-dimensional solids is present in one dimension. An important result of this approach is that we are able to observe how the bulk behavior is obtained for the center of the one-dimensional chains and how this behavior changes as the ends of the chain are approached. A realistic situation of a 1-D cluster can be found in current studies of nanotechnology systems where a 1-D chain of atoms is actually used in single-molecule conductivity experiments. To study the connection of a 1-D chain to an interface, we must know how the atoms from the ends differ from the central atoms.

We report a systematic DFT study of copper chains from 2 to 15 atoms, as well as several planar structures, and two three-dimensional systems. All these clusters were fully optimized, and we examine average bond energies, electronic structure, spin density, and ionization potentials. Although we do not expect to obtain bulk properties from these small 2 or 3-D clusters, a semiempirical formula is used to get some insights into the connection between the clusters ionization potentials and the bulk work function.

2. Methodology

We have used density functional theory (DFT) techniques,[25−31] combined with effective core potentials. Presently, this seems to be the most powerful combination of tools to deal with a relatively large number of big atoms. The basis set used for the copper atom is the Los Alamos National Laboratory set (LANL) for effective core potentials (ECP) of double-ζ type.[32,33] It consists of a small core ECP with 3s and 3p orbitals in the valence space. The use of DFT is fully justified due to the fact that it is an ab initio tool able to deal with a broad variety of systems. The functional that we used is the B3PW91.[34−37] All calculations were performed using the Gaussian-94 program.[38] Full geometry optimizations were performed via the Berny algorithm in redundant internal coordinates.[39] The thresholds for convergence were 0.00045 au and 0.0003 au for the maximum force and root-mean-square (RMS) force, respectively. The self-consistency of the noninteractive wave function was performed with a requested convergence on the density matrix of 10^{-8} and 10^{-6} for the RMS and maximum density matrix error between iterations, respectively. These settings provide correct energies of, at least, five decimal figures and geometries of approximately three decimal figures within the level of theory. On the other hand, the use of the pseudopotentials with relativistic corrections has been widely demonstrated to be a good compromise with the alternative use of full-electron procedures. This reduces the required computational effort without loss of accuracy.[40] In summary, the only restriction imposed in our calculations is the use of a neon core for copper atoms; nevertheless, this is not a strong restriction because in the formation of molecular orbitals and energy bands the external orbitals are involved while the inner remain practically unchanged. However, relativistic corrections for the Cu atoms are considered in the ECP.

3. Results and Discussion

DFT calculations used in this work yield the electronic structure, geometry, and ionization potential (IP) of several one-, two-, and three-dimensional Cu cluster systems. As described in the Introduction, the reason for this systematic procedure lies on the fact that one can extract the physics of the evolution of the system beginning from the 1-D case, even though for clusters of more than two atoms the linear structures are not the most stable. The selection of initial geometries was based on specific known properties of bulk copper. However, the final structures always corresponded to a minimum energy configuration of the cluster. The structure of crystalline Cu corresponds to a face-centered cubic (fcc) lattice, with a cube side of 3.615 Å and a distance from the vertex to the face-centered atom of 2.556 Å. Planar and 3-D clusters in this study correspond to either the (111) or (100) planes. We first analyze one-dimensional (1-D) chains containing up to 15 copper atoms. Then, we examine models of the (111) and (100) planes (2-D) and finally two three-dimensional (3-D) structures containing the (100) and (111) planes, respectively. We determine the ground-state multiplicity by optimizing the three lowest multiplicities of each chain and planes. For all geometric structures, the ground state of the neutral and first ionized states corresponded to their lowest multiplicity.

3.1. One-Dimensional Chains. Table 1 shows the bond lengths of the *n*-atom chains. For each value of *n*, the bond lengths are indicated from the end-atom toward the center of the chain. Bond lengths alternate and are reminiscent of a conjugated chain. This conjugate character may have a strong relevance regarding the conductivity properties of Cu. The bond lengths between any pair of central atoms in the cluster tend to a value of 2.36 Å. This value is closer to the 2.556 Å distance between a face-centered and a vertex atom than to the 3.615 Å cube side distance of the experimental copper fcc cubic lattice. On the other hand, the evolution of the linear chain end bond lengths with the increase of the number of atoms in the cluster provides insights regarding the tendencies toward bulk behavior.

Figure 1 shows the end and next-to-end bond lengths for even and odd chains, respectively. The shortest bond length corresponds to the chain ends, since they only have one first neighbor. The bond lengths for the even and odd clusters practically converge to the same bond distances, although each set of clusters has very different values for the smallest clusters. Figure

TABLE 1: Optimized Bond Lengths and Absolute Energies of *n*-atom Linear Clusters

n	bond lengths (Å)							energy (Hartrees)	number of imaginary frequencies
1								−196.15426	
2	2.256[a]							−392.37925	0
3	2.330							−588.56691	2
4	2.285	2.419						−784.77586	4
5	2.313	2.374						−980.96948	4
6	2.291	2.411	2.313					−1177.17431	8
7	2.305	2.387	2.352					−1373.37037	10
8	2.294	2.407	2.318	2.398				−1569.57325	12
9	2.303	2.392	2.344	2.364				−1765.77064	14
10	2.295	2.407	2.321	2.394	2.324			−1961.97236	16
12	2.296	2.407	2.323	2.392	2.328	2.388		−2354.37156	20
15	2.301	2.397	2.337	2.375	2.349	2.365	2.358	−2942.97021	24

[a] The experimental value is 2.22 Å.[43]

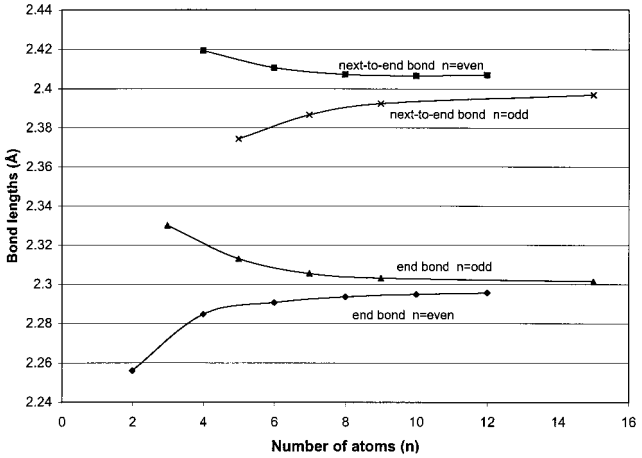

Figure 1. Bond lengths of the end and next-to-end bonds in the linear chains. Notice that the even and odd chains converge to the same bond lengths.

1 illustrates that the end bond lengths tend to 2.3 Å, while the next-to-end bond lengths tend to a value close to 2.4 Å. A similar behavior can be predicted for the other bonds by analyzing the evolution of the bond lengths in the third and successive columns of Table 1. Table 1 also shows that, as the number of atoms in the chain increases, the central bond length tends to a value of 2.36 Å. Therefore, strong effects due to truncation of the chain are reflected primarily on the end bond lengths.

It is interesting to relate these observations to changes in the electronic structure due to the formation of the chain. We have examined the s, p, and d character for each atom, which for isolated Cu atoms should be $s^3\ p^6\ d^{10}$ considering only the valence orbitals. Table 2 shows these results for chains of 4, 5, 9, and 10 atoms. The end atoms are the closest to a $s^3\ p^6\ d^{10}$ occupation, while in the central atoms, some of the s character is lost and the p character is enhanced. The d character is less affected by the atomic position, although a small change is also observed between the end and central atoms. These features cannot be captured with a simple extended Huckel calculation[41,42] that yields a more homogeneous distribution and lead to opposite conclusions with respect to charge distribution as discussed in a latter section with relation to the three-dimensional structures. Note also that, when the number of atoms in the chain increases, the end effects in the electronic structure are more pronounced. These 1-D cluster calculations corroborate quantitatively that the ends of the cluster have different geometric and electronic structure than the bulk. Therefore, cluster calculations are actually needed for an acceptable, atomic level description of the ends. Those effects would be lost in typical energy band calculations. The large change of more than 0.1 Å observed between the two initial bonds in the 1-D chains suggests that a similar behavior can be expected at the surface of a crystal, where the surface bonds must be structurally different than the inner equivalent bonds. According to the trend shown by the bond lengths in Table 1 and the population distribution from Table 2, we infer that this effect will be present in an infinite chain and an equivalent behavior will be present for surface atoms with respect to internal or bulk atoms in a 3-D system. Since the ends are far different from the bulk, we have a compelling justification for the use of clusters instead of bulk representations of a metal surface to evaluate both local surface phenomena and surface chemistry details that can be revealed only with a full electronic treatment.

TABLE 2: Population Character for Clusters of 4, 5, 9, and 10 Atoms[a]

atom	S	P	D
	4-atom chain		
1	2.947	6.063	9.940
2	2.775	6.366	9.908
	5-atom chain		
1	2.958	6.068	9.938
2	2.724	6.330	9.906
3	2.803	6.441	9.907
	9-atom chain		
1	2.937	6.063	9.939
2	2.728	6.312	9.905
3	2.782	6.406	9.907
4	2.756	6.347	9.907
5	2.791	6.325	9.906
	10-atom chain		
1	2.937	6.061	9.939
2	2.741	6.298	9.906
3	2.764	6.412	9.908
4	2.771	6.338	9.907
5	2.776	6.332	9.907

[a] Only half of the atoms in each chain are shown.

To check the precision of our DFT results, we have compared some of the properties of the smallest clusters to experimental values. The calculated equilibrium distance for the dimer, 2.256 Å, compares well with the experimental value, 2.22 Å.[43] Its calculated vibrational frequency, $\omega_e = 255.5\ cm^{-1}$ is also in very good agreement with the 265 cm^{-1} obtained experimentally.[43] Our results represent a major improvement over local density approximation (LDA) calculations, 2.18 Å and 292 cm^{-1} for the equilibrium distance and vibrational frequency, respectively.[44] The calculated values for the anion Cu_2^-, 2.37 Å for the equilibrium distance and 198 cm^{-1} for the stretching mode, compare very well with 2.34 Å and 210 cm^{-1} found experi-

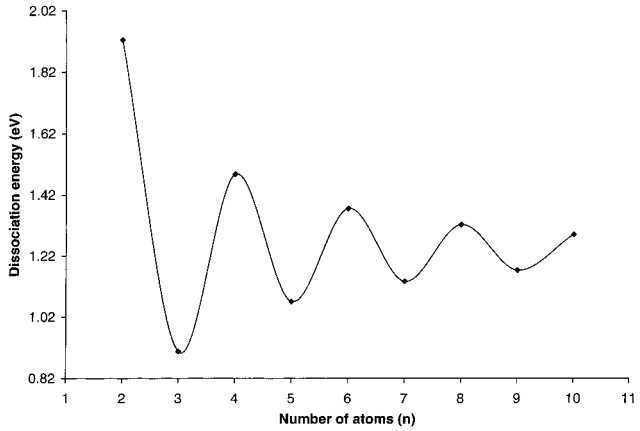

Figure 2. Dissociation energy: $Cu_n \rightarrow Cu_{n-1} + Cu$.

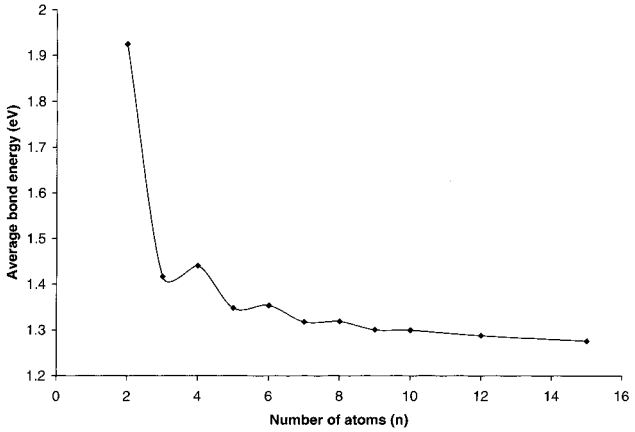

Figure 3. Average bond energy vs number of atoms in the linear chains.

mentally.[43] Again, an improved agreement compared to previous LDA calculations, of 2.26 Å and 227 cm^{-1}.[44] The calculated electron affinity for the copper dimer is 0.62 eV, while the experimental value is 0.84 eV.[43]

The absolute energies obtained for the linear clusters are listed in Table 1. They resulted from full geometry optimizations. However, except for the dimer, which corresponds to the ground state, the solutions correspond to local minima, or to transition states, since clusters of three or more atoms tend to arrange in bent geometries.[45,44] Thus, the vibrational modes corresponding to bending are unstable, while the stretching modes along the direction of the line are stable, which preserves the validity of our conclusions.

Figure 2 shows the dissociation energy of one atom from an *n*-atom chain,

$$D_e = (E_{n-1} + E_1) - E_n$$

where E_i is the energy of the system with *i* atoms. It is observed that the dimer system is the most stable, which also explains the tendency of the chain to get conjugated. It takes more energy to extract one atom from the even chains than from the odd ones, because in the even chains all electrons are paired and the bond strength is at maximum, while in the odd chains not all electrons are paired. The calculated dissociation energy for the dimer, 1.92 eV, is in excellent agreement with the measured value of 1.96 eV.[43]

The relative stability can be also evaluated through the average energy per bond as a function of the number of atoms defined as

$$\tilde{D}_e = (nE_1 - E_n)/(n-1)$$

This average bond energy shown in Figure 3 confirms the stability of the dimer and again illustrates the oscillation between even and odd-number chains, however more attenuated than the dissociation energy because of the averaging effect. Another property whose behavior is implicit in Figure 3 is the atomization energy, ΣD_e

$$\Sigma D_e = (n-1)\tilde{D}_e$$

It is defined as the product of the average energy per bond times the number of bonds, and the values are listed in Table 3.

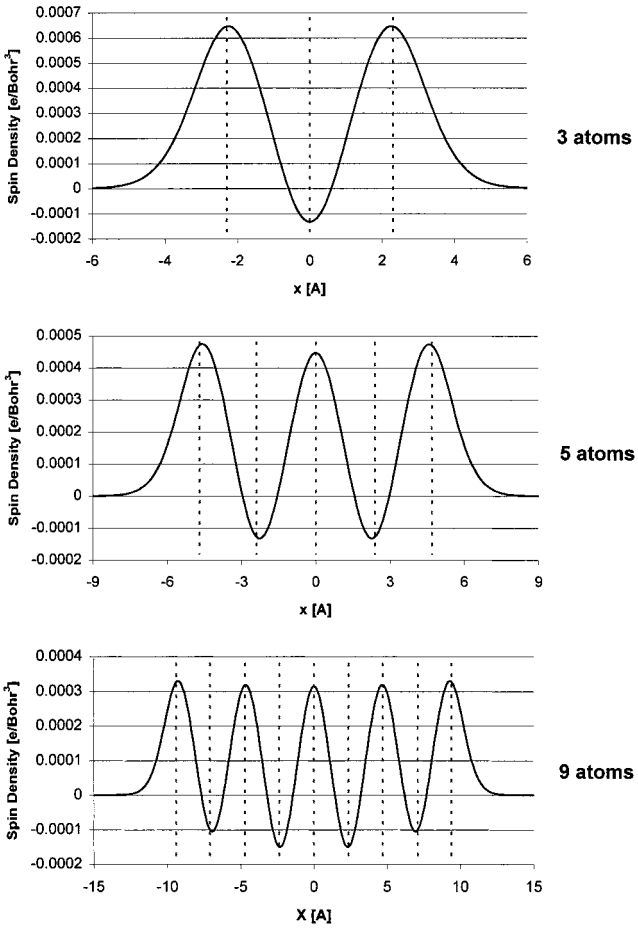

Figure 4. Spin density for chains of 3, 5, and 9 atoms along a line parallel to the chain axis, at 2 Å. Vertical lines indicate the nuclei positions.

The differences between even and odd clusters can be further analyzed by studying the spin-density distribution of the odd chains, illustrated in Figure 4 for chains of 3, 5, and 9 atoms. The same periodic behavior observed for the electronic and geometric properties is also reflected on the spin distribution of odd chains. The spin density difference between α and β states, displayed along a parallel line at 2 Å from the chain axis, arranges in regions of maximum density at the ends of

TABLE 3: Atomization Energies (ΣD_e) of Linear Chains

number of atoms	2	3	4	5	6	7	8	9	10	12	15
ΣD_e	1.92	2.83	4.32	5.39	6.77	7.90	9.23	10.4	11.69	14.16	17.86

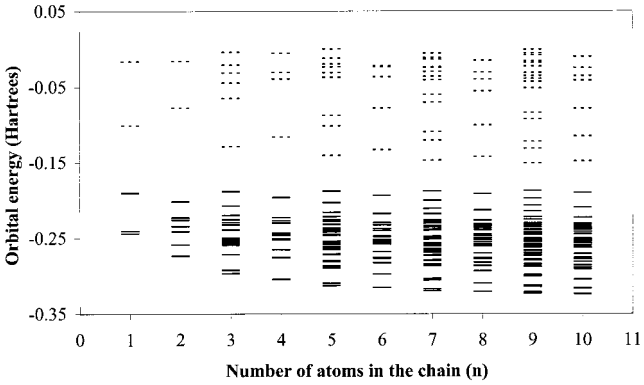

Figure 5. Occupied (continuous line) and unoccupied (dashed line) energy levels of linear Cu chains (energies in the neighborhood of the HOMO and LUMO are shown).

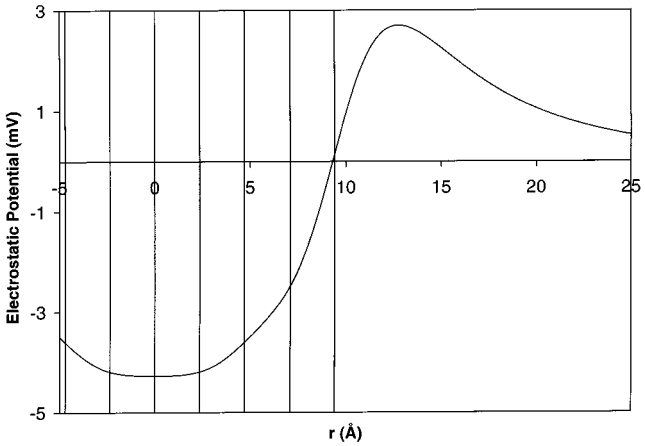

Figure 6. Electrostatic potential of the nine-atom chain, calculated in a direction parallel to the axis at 5 Å from the chain. Vertical lines represent the position of the nuclei of seven out of nine atoms. The curve is symmetric and the origin is at the center of the chain.

the chain, alternating with minima toward the center. Note that the spin distribution becomes more homogeneous as the number of atoms increases; however, the end effects become more pronounced. The results for the trimer shown in Figure 4 are in total agreement with results from electron spin resonance spectrum measured for this system.[46]

Another indication of the evolution from the molecular cluster to the metal state is given by the energy gap between the highest occupied and the lowest unoccupied energy levels. As the number of atoms in the cluster increases, the atomic levels gradually loose their identity to form the well-known band structure where the electrons have practically a continuum of energy levels rather than discrete energy levels. Figure 5 depicts the HOMO and LUMO and their nearest energy levels corresponding to each linear cluster. There is an initial oscillation of the HOMO energy with respect to the number of atoms in the chain, this oscillation decays as the HOMO and tend to LUMO constant values for the larger chains. The even clusters have lower HOMO energy and higher LUMO energy than the odd clusters. Therefore, the former clusters are more stable than the latter, but this difference in stability becomes negligible as the number of atoms in the chain increases. The HOMO−LUMO gap oscillates but tends to decrease for the largest systems, where the highest occupied levels will conform the valence band and the lowest unoccupied levels the conduction band.

Mulliken population analysis provides an estimate of the distribution of charges.[47] Table 4 displays the charge for atoms from one end to the center of the chain. The electrons tend to concentrate at the center of the chain giving an electron-deficient structure at the ends. As observed with other properties, when the number of atoms in the chain increases, the distribution of charges is such that the end effects become more pronounced. However, this could be just an artifact of the Mulliken population analysis since the central atoms have more basis functions available to represent their charge. Therefore, we used a better indicator of the real charge distribution, the electrostatic potential $V(r)$, given by the expression[48]

$$V(\vec{r}) = \sum_{A=1}^{n} \frac{Z_A}{|\vec{R}_A - \vec{r}|} - \int \mathrm{d}\vec{r}' \frac{\rho(\vec{r}')}{|\vec{r} - \vec{r}'|}$$

Where ρ is the electron density assumed positive, and R_A is the position of the nucleus A, Z_A is the atomic charge of nucleus A, and n is the total number of nuclei in the system. The density, ρ, which is the same for the interacting and noninteracting systems in DFT, is calculated simply from the noninteracting wave function ψ as follows:

$$\rho(\vec{r}) = N \int\int \ldots \int\int \mathrm{d}\vec{r}_2 \mathrm{d}\vec{r}_3 \ldots \mathrm{d}\vec{r}_{N-1} \mathrm{d}\vec{r}_N |\psi(\vec{r}, \vec{r}_2, \vec{r}_3, \ldots, \vec{r}_{N-1}, \vec{r}_N)|^2$$

where N is the total number of electrons in the system. Figure 6 shows the electrostatic potential parallel to a nine-atom chain, the vertical lines indicate the location of seven of the nine chain atoms, where the origin is at the center of the symmetric chain. The calculation was done at 5 Å in a direction parallel to the chain. In agreement with the Mulliken population analysis, the values of the electrostatic potential suggest that the center atoms bear an effective negative charge, while the ends become slightly positive.

3.2. Two-Dimensional Systems. Table 5 shows fully optimized geometries and energies of planar Cu clusters illustrated in Figure 7. **7A** and **7B** resemble the geometrical arrangement of the (111) plane, although the optimized bond lengths for the

TABLE 4: Mulliken Population in the Linear Chains

n	Mulliken charges (au)							
2	0							
3	0.023	−0.047						
4	0.049	−0.049						
5	0.035	0.040	−0.151					
6	0.041	0.048	−0.089					
7	0.052	0.048	−0.099	−0.001				
8	0.059	0.047	−0.097	−0.009				
9	0.061	0.055	−0.094	−0.011	−0.023			
10	0.063	0.055	−0.085	−0.017	−0.016			
12	0.066	0.056	−0.083	−0.008	−0.006	−0.025		
15	0.068	0.061	−0.084	−0.003	−0.011	−0.012	−0.016	−0.007

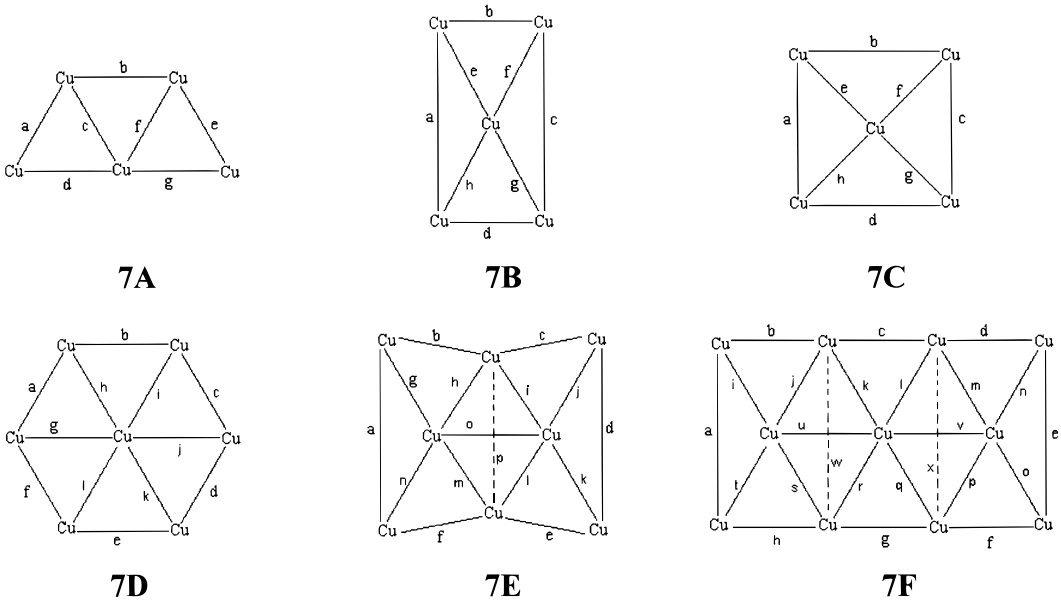

Figure 7. Geometries of planar structures. Optimized bond lengths are included in Table 5.

TABLE 5: Optimized Properties of Planar Structures

structure	bond lengths (Å)	energy (Hartrees)	average bond energy (eV)	atomization energy (eV)	HOMO (eV)	LUMO (eV)
7A	$a = 2.414$ $b = 2.464$ $c = 2.444$ $d = 2.399$ $e = 2.412$ $f = 2.451$ $g = 2.406$	−981.0336	−1.02	−7.14	−4.53	−2.04
7B	$a = 4.097$ $b = 2.402$ $c = 4.097$ $d = 2.404$ $e = 2.375$ $f = 2.375$ $g = 2.374$ $h = 2.374$	−981.0167	−0.83	−6.68	−4.07	−2.18
7C	$a = 3.234$ $b = 3.234$ $c = 3.234$ $d = 3.234$ $e = 2.274$ $f = 2.299$ $g = 2.274$ $h = 2.998$	−980.9798	−0.71	−5.67	−4.67	−2.29
7D	$a = 2.419$ $b = 2.548$ $c = 2.423$ $d = 2.419$ $e = 2.425$ $f = 2.424$ $g = 2.426$ $h = 2.480$ $i = 2.483$ $j = 2.425$ $k = 2.481$ $l = 2.483$	−1373.4835	−0.91	−10.98	−3.79	−2.74
7E	$a = 4.452$ $b = 2.389$ $c = 2.389$ $d = 4.448$ $e = 2.389$ $f = 2.389$ $g = 2.406$ $h = 2.491$ $i = 2.489$ $j = 2.406$ $k = 2.406$ $l = 2.489$ $m = 2.492$ $n = 2.406$ $o = 2.930$ $p = 4.028$	−1569.7167	−1.01	−13.13	−4.82	−2.71
7F	$a = 4.276$ $b = 2.424$ $c = 2.517$ $d = 2.423$ $e = 2.482$ $f = 2.423$ $g = 2.517$ $h = 2.424$ $i = 2.403$ $j = 2.485$ $k = 2.447$ $l = 2.445$ $m = 2.481$ $n = 2.401$ $o = 2.403$ $p = 2.486$ $q = 2.446$ $r = 2.446$ $s = 2.485$ $t = 2.401$ $u = 2.589$ $v = 2.594$ $w = 4.197$ $x = 4.193$	−2158.3836	−0.85	−18.68	−4.18	−2.73

first structure, and the *b*, *d*, *e*, *f*, *g*, and *h* bond lengths in the second, are shorter than the characteristic (111) distance, 2.556 Å. The distribution of atoms in **7C** is similar to that in the (100) plane, although the optimized geometric parameters (Table 5) are contracted with respect to those in Cu metal. The optimized *a*, *b*, *c*, and *d* distances are shorter than the bulk fcc of Cu bond

length 3.615 Å, and the *e*, *f*, *g*, and *h* distances are shorter than the 2.556 Å diagonal face bond. These bond length contractions are a consequence of the decrease in the coordination number of the atoms in the respective clusters compared to the bulk values and resemble the behavior found with the end bond lengths in the 1-D systems. From all the five-atom planes, **7A** has the lowest average bond energy, as indicated in Table 5. This is in agreement with previous LDA calculations.[44] **7A** is also the only five-atom structure where all vibrational modes were found real. **7B** and **7C** have two and one imaginary vibrational modes, respectively. One of the unstable modes in **7B** is on the plane and one is perpendicular to it. The existence of the former suggests that **7B** would evolve to **7A**, while the latter, which is the most intense, suggests the existence of a nonplanar minimum energy structure. One in-plane mode was found unstable for **7C**.

Other three planar structures were built adding atoms to **7A**. These structures are **7D**, **7E**, and **7F** containing 7, 8, and 11 copper atoms. Their bond lengths, shown in Table 5, are closer to the (111) characteristic distance than those from the five-atom clusters. The minimum energy state corresponding to the eight-atom plane, **7E**, is a singlet, while all the minimum energy states corresponding to the other planar geometries are doublets. In agreement with the analysis done on the 1-D systems, the eight-atom system yields higher stability compared to the odd clusters, as observed from the calculated average energy per bond from Table 5.

All 2-D systems yielded a distribution of charges with a common feature. The atom with the highest coordination number is negatively charged, and all the others are positively charged. This behavior resembles linear clusters, where chain ends become slightly positive while the inner atoms bear small negative charges. **7F**, an 11-atom cluster, has a central atom with coordination number 6 that has an effective charge of -1 according to the Mulliken population analysis. The two middle row neighbors to this central atom, each one coordinated to five atoms, are positively charged ($\sim$0.5). In contrast with the previous clusters, the two central atoms in the top and bottom rows, with coordination number 4, bear small positive charges, and the ones at the corners, with coordination number 2, bear small negative charges. However, the absolute value of these charges is so small that all the atoms in **7F**, except those in the middle row, can be considered neutral.

The distribution of spin density for a parallel plane at 2 Å from the trapezoidal structure **A** is displayed in Figure 8. Two regions of high spin density are shown as isodensity contours in Figure 8a, while Figure 8b indicates the atomic positions. The nonuniformity in the distribution is associated with the geometric characteristics, which in turn are determined by hybridization of the *3*d and *4*s orbitals. The energies corresponding to the HOMO and LUMO are included in Table 5. Both, the HOMO and LUMO energies of the planar structures are lower than those in the linear systems with the same number of atoms. However, the HOMO−LUMO gap, which can be considered an indication of the cluster to metal evolution, is higher in 2-D than in 1-D systems of the same number of atoms. In the one-dimensional system, there is a Peierls distortion and the system is heavily dominated by overlap considerations.[49] The overlap from the central atom to the end atom is approaching zero for a chain length of 15. This corresponds to an interaction between Cu atoms separated roughly by 8 atoms. For the 2-D cases studied here, no atom is more than four Cu atoms away from each other. There is still overlap, and the HOMO/LUMO gap is larger.

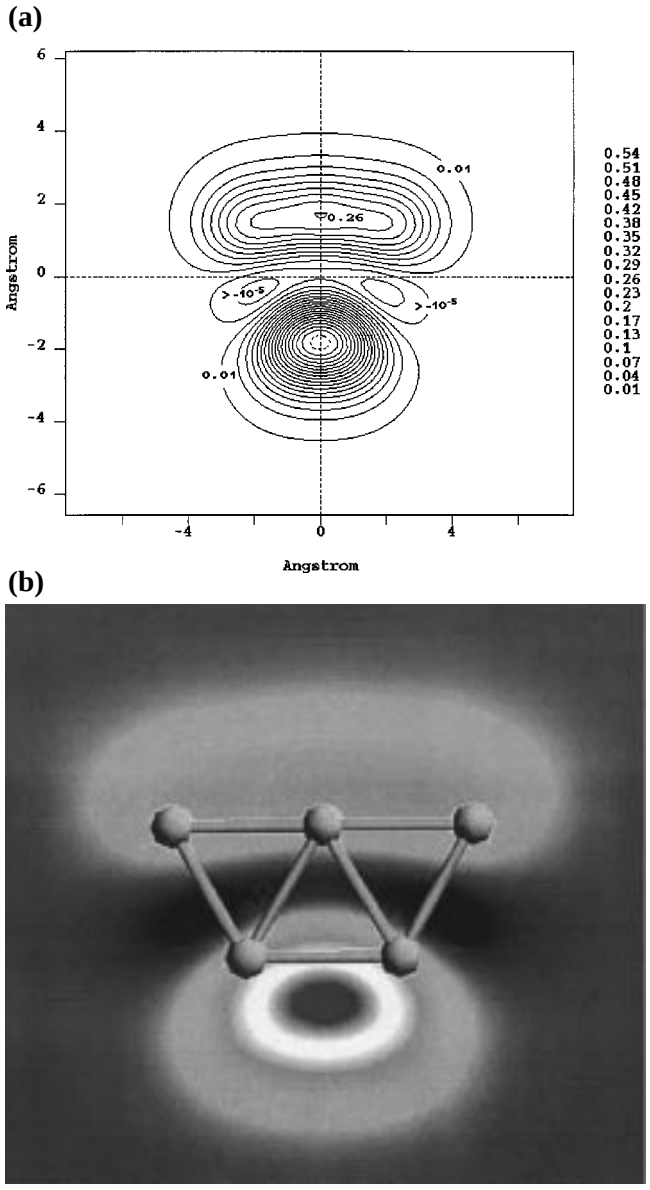

Figure 8. (a) Contours of spin density corresponding to structure **A** in Figure 7. Isodensities are calculated on a plane parallel to the plane of the atoms, at 2 Å. Spin densities decrease from each of the central contours outward according to the scale. The density inside the dashed contour is 0.54. (b) Same as (a), indicating the atomic positions.

3.3. Three-Dimensional Systems. The fcc unit cell of Cu was studied considering two different surfaces, one along the (100) and another along the (111) plane. In both cases, the initial bond lengths and angles were those in the experimental fcc copper crystal lattice. Figure 9 displays a fully optimized cubic structure **(9A)** corresponding to the (100) face. After optimization, the distances between atoms became shortened with respect to the experimental distances in the bulk metal. Thus, the bond length between vertexes decreased from 3.615 to 3.477 Å, and the distance from a vertex to a face-centered atom decreased from 2.556 to 2.462 Å. The distance between two face-centered atoms belonging to adjacent faces increased from 2.556 to 2.614 Å, while the distance between two face-centered atoms of opposite faces increased from 3.615 to 3.697 Å. The fcc geometry in **9A** is not totally symmetric, but equivalent bonds or distances differ at most in the third decimal figure. As it was observed in the 1-D and 2-D systems, the net negative charges tend to concentrate on the face-centered atoms with highest coordination number, while atoms in the vertexes bear

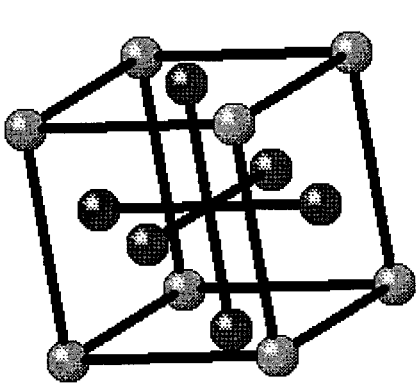

9A

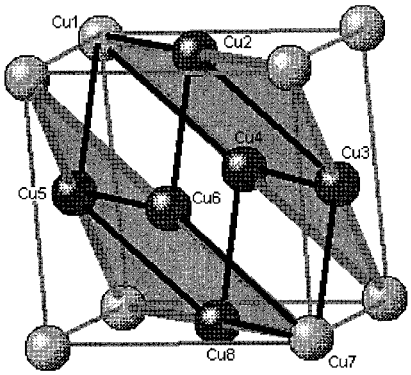

9B

Figure 9. Geometries of three-dimensional structures. Optimized bond lengths and angles for structure **B** are indicated in Table 6.

TABLE 6: Optimized Bond Lengths and Angles Corresponding to 3-D Structure 9B[a]

bond	bond lengths (Å),
1−2	2.417
2−3	2.395
3−4	2.394
4−1	2.418
5−6	2.393
6−7	2.419
7−8	2.417
8−5	2.395
1−5	2.395
2−6	2.419
3−7	2.395
4−8	2.418
1−8	3.831
2−7	3.827
1−7	4.528
2−8	4.528
3−5	2.854
4−6	4.508
angle	**angle measure (deg)**
1−4−3	75.050
2−3−4	105.667
1−2−8	104.213
3−4−8	75.050

[a] Atom numbers are displayed in Figure 9.

slightly positive charges. These conclusions differ from those derived from self-consistent extended Huckel calculations[42] performed on Cu clusters of 16 and 19 atoms which yielded highest electronic density for the atoms located in the middle of the cluster (7 nearest neighbors), while center (12 nearest neighbors) and end atoms (4 nearest neighbors) were found slightly positive.

A second 3-D structure representing the (111) face was built based upon the (111) planes shown in **9B** (Figure 9). This parallelepiped structure consists of four atoms from each (111) plane. Two different types of bonds are present, those between a vertex and a face-centered atom, and those between two face-centered atoms. The corresponding experimental value in both cases is 2.556 Å. After optimization, these bond lengths are reduced to 2.395 and 2.418 Å, respectively. Distortions from a symmetric structure are more pronounced in this case. Table 6 shows the optimized bond lengths and angles corresponding to this structure. Each of the two atoms (1 and 7) located at the vertexes of **9B** are bonded to three face-centered atoms with bond lengths of 2.395 Å. They bear relatively high positive charges (0.18), while all the other atoms are negatively charged (−0.06). Atoms 1 and 7 of **9B** are the ones located farthest from each other, which reduces their coordination number with respect to the face-centered atoms; therefore, these observations agree with the correlation found in the previous cases between the coordination number and the charge associated with a given atom. Between the two 3-D structures, **9A** is found the most stable based on the average energy per bond shown in Table 7. The HOMO−LUMO gaps are 1.72 and 1.90 eV for **9A** and **9B**, respectively. This second value is slightly lower than the one for the eight-atom planar structure, 2.11 eV, however is higher than that for the 1-D case, 1.33 eV.

TABLE 7: Optimized Properties of 3-D Structures

structure	energy (Hartrees)	average bond energy (eV)	atomization energy (eV)	HOMO (eV)	LUMO (eV)
9A	−2747.1434	−1.03	−26.77	−4.57	−2.85
9B	−1569.7215	−0.95	−13.26	−4.49	−2.58

Experimental and theoretical results indicate that the cluster binding energy per atom, E_b, calculated as follows:

$$E_b = (nE_1 - E_n)/n$$

evolves toward the metal cohesive energy for a sufficiently large number of atoms. For copper, the experimental cohesive energy is 3.50 eV.[50] We found values of 1.19 eV for the 15-atom chain, 1.70 eV for planar structure **7F**, and 1.91 and 1.66 eV, respectively, for the 3-D structures **9A** and **9B**. Thus, the highest value of the binding energy per atom found for the 14-atom 3-D cluster is slightly larger than 50% of the bulk cohesive energy of the metal.

9A and **9B** have singlet multiplicities. To investigate the existence of a ground state of higher multiplicity, we have performed single-point calculations on the singlet optimized geometries, for $m = 3$ and $m = 5$. Although we have not fully optimized the geometries corresponding to the triplet and quintet, we found that the calculated single-point energies of the higher multiplicities differ in substantial amounts from that of the singlet state, suggesting that the ground state of these clusters is a singlet.

3.4. Ionization Potential. The ionization potential (IP) is defined as the difference between the ground state energies of the neutral and its first ionized state. Thus, the definition of IP agrees with that of the WF, which should be the IP of the infinite system. However, even in the infinite system, the IP and the WF will be numerically different except if the WF is measured on the surface where the highest occupied orbital is located. The term ionization potential is generally used for molecules

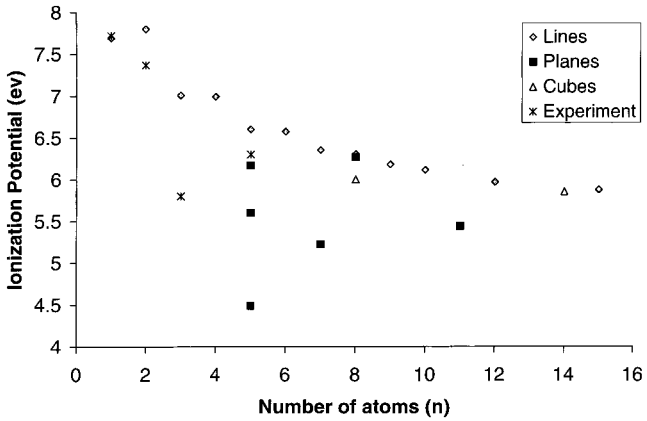

Figure 10. Ionization potentials vs number of atoms for 1-, 2-, and 3-D systems. Correspondence with structures is indicated in Table 8. Experimental values are included.[54]

or small clusters, where the HOMO is delocalized around the whole system, while WF is reserved for the bulk and depends on specific surfaces. Two quantities can be defined in relation to experimentally measured IP values: (1) the adiabatic IP is the difference between the neutral system and the ion when both are in their respective ground state, taking into account the relaxation of the ion that follows the emission of the electron, and (2) the vertical IP is the difference between the neutral system and the ion, both at the geometrical configuration of the neutral ground state. Therefore, depending on the experimental setup, measured values of the WF may correspond to the vertical or the adiabatic IP. Following the former definition, the WF coincides with the vertical IP, the energy released when fully relaxing the ionized system is not included to compute the energy needed to extract an electron.

Figure 10 shows the calculated vertical IP for the linear clusters in comparison to those for the 2- and 3-D clusters, vs the number of atoms in the system. To test the effect of the ECP in the description of our system, we have calculated the IP for the single Cu atom and for the dimer using a full-electron DFT calculation with the modified Wachters basis set.[51] For the single atom and the dimer, the IPs agree well with the experimental values.[52] The atomic IP given by the full electron calculation is 7.88 eV, compared to 7.69 eV (ECP) and 7.73 eV (experimental). For the dimer, the three values are 7.89 eV (full-electron), 7.80 eV (ECP), and 7.37 eV (experimental).[52] Oscillations in the IP are characteristic of monovalent metal clusters reflecting the behavior of closed- versus open-shell systems and the nature of pair occupation of the valence electron into the molecular orbitals, and have been reported in many experimental and theoretical investigations.[17,15,53] The IP tends to a constant value estimated in 5.8 eV for the 1-D system. As illustrated in Figure 10, planar and 3-D clusters have IPs lower than or equal to the corresponding value for the chain with the same number of atoms. The most stable planar pentamer **7A** has an IP of 6.17 eV, in good agreement with the experimental value of 6.30 eV.[54]

To investigate the connection of the calculated IP for clusters with the bulk WF we examined an expression based on the concept of effective coordination number introduced by Zhao et al.[55,56] This equation was proposed to calculate cluster ionization potentials when the WF for the bulk is known. The results of this model showed very good agreement with experiments for several cluster sizes where other commonly used models such as the conducting-sphere-droplet approximation failed.[55,56] The expression given by Zhao et al. for the IP of the *n*-atom cluster is

$$\mathrm{IP}_{\mathrm{Cu}_n} = \mathrm{IP}_{\mathrm{Cu}_1} - (\mathrm{IP}_{\mathrm{Cu}_1} - \mathrm{WF})\sqrt{\frac{Z_{\mathrm{Cu}_n}}{Z_{\mathrm{bulk}}}}$$

where $\mathrm{IP}_{\mathrm{Cu}_n}$ is the ionization potential for a *n*-atom cluster, Z_{Cu_n} is the coordination number of the cluster, and Z_{bulk} is the coordination number for the bulk. The first term is the noninteracting electron contribution, and the second term is proposed to reflect variations in the IP of the *n*-atom cluster with respect to the bulk work function due to finite size effects. Since we are able to determine precisely the cluster IP, we invert the expression to obtain an estimate of the WF. We used bulk coordination numbers Z_{bulk} of 2 for the 1-D system, 4 and 6 for the (100) and (111) 2-D systems, respectively, and 12 for 3-D systems. The criteria adopted for the estimation of the coordination number Z_{Cu_n} of each site was counting as first neighbors only those that would exist in the bulk crystal. However, as was mentioned above, many of the characteristic unit cell dimensions get reduced for the finite system. Therefore, in some cases, the distinction between first and second neighbors becomes less apparent. Cluster coordination numbers calculated as an average based on the arithmetic mean are shown in Table 8, along with the calculated IP and extrapolated WF values.

For the 1-D system, the variation of the extrapolated WF with respect to the IP is very small. Since the coordination number of an *n*-atom chain rapidly tends to the bulk 1-D value, the extrapolated WF converges to a limit of about 5.8 eV. The most stable planar systems, **7A** and **7E**, yield the highest IP and extrapolated WF values. The 2-D case depends more extensively on the specific structure, and a 2-D limit for the WF cannot be inferred from these data.

Reported experimental values of the WF are 4.59, 4.48, 4.94, and 4.53 eV for the (100), (110), (111), and (112) planes, respectively, yielding an average of 4.64 eV.[57] The last set in Table 8 corresponds to 3-D structures. The (100) structure, **9A**, yields higher extrapolated WF than the one corresponding to a (111) plane **9B** while their IPs follow the opposite trend, which is in agreement with experimental results. The wrong trend of

TABLE 8: Calculated DFT Ionization Potentials and Extrapolated Work Function (see text) for 1-, 2-, and 3-D Clusters

	no. of atoms											
	1	2	3	4	5	6	7	8	9	10	12	15
IP (eV)	7.69	7.80	7.00	6.99	6.60	6.57	6.35	6.31	6.18	6.11	5.97	5.88
cluster coord. no.	0	1.0	1.33	1.5	1.6	1.67	1.71	1.75	1.78	1.8	1.83	1.87
WF (eV)	–	7.84	6.86	6.88	6.47	6.46	6.25	6.21	6.09	6.03	5.89	5.81

	structure							
	7A	7B	7C	7D	7E	7F	9A	9B
IP (eV)	6.17	5.60	4.48	5.22	6.27	5.44	5.85	5.99
cluster coord. no.	2.8	2.4	1.6	3.4	3.2	3.6	5.2	3.5
WF (eV)	5.46	4.38	2.63	4.41	5.74	4.78	4.88	4.54

the extrapolated WF may be due to the nature of the approximation used and to uncertainties in the estimation of the coordination numbers. However, the average WF for the (100) and (111) planes is 4.71 eV. This value compares reasonably well with the average experimental number and supports the concept of the local work function.

Tables 7 and 8 illustrate the difference between the extrapolated WF and the negative of the HOMO values, which are often taken as the WF. It has been proved that, when an exact functional is used, the negative of the HOMO energy should be exactly equal to the vertical IP.[58] Such an exact functional has not yet been developed. In the meantime, the use of an effective coordination number in a significant number of 3-D structures should provide useful insights into the effects of structural changes on the local work function. Work is in progress to test the sensitivity and validity of these findings to metal substitution, vacancies, or other defects in catalysis and reaction processes at interfaces.

4. Conclusions

A systematic study of Cu clusters has been performed using DFT techniques combined with effective core potentials. The evolution of several properties such as dissociation energy, HOMO−LUMO gap, and ionization potential is analyzed as the system evolves toward "bulk" in one, two, and three dimensions. The one-dimensional model is used as the starting point, because it is very likely that this is the only case where one can observe the cluster to bulk evolution of properties with the current computational resources.

For the 1-D systems, it is found that the dissociation energy and ionization potential follow an oscillatory behavior that reflects a conjugate-like character indicative of the pair-occupation nature of copper. Calculated bond lengths, vibrational modes, ionization potentials, and dissociation energies for the smallest clusters agree very well with the available experimental information. A 1-D limit is rapidly reached by a chain system of 15 atoms. Most of the analyzed properties show substantial differences between the end atoms and those occupying central locations. The chain central atoms, having larger coordination numbers than the end atoms, bear the highest negative charge. The same feature is observed in planar and 3-D structures for the highest coordinated atoms. The ends or low-coordinated atoms tend to concentrate the spin density.

A semiempirical expression dependent on the cluster average coordination number is used to investigate the connection between the calculated cluster ionization potential and the local work function for all the clusters in this study. Although only trends were expected from the empirical formula, we can detect the effects of local variations on the work function determined by the cluster local coordination numbers. In fact, this is an important point for understanding heterogeneous catalysis, where defects or local variations on surfaces are made responsible of changes in the expected reaction rates. This study shows that for certain properties the local effects are more important than the bulk effects and therefore, the use of clusters is a proper choice to represent a surface.

Acknowledgment. We are indebted to one of the referees for very helpful comments and suggestions. P.B.B. is thankful for financial support from NSF Grant CTS-9720537 and computer resources from Pittsburgh Supercomputer Center through Grant CHE 970009P, and from NCSA Grant DMR990000N to P.B.B. and P.A.D. J.M.S. acknowledges ONR and DARPA for financial support and NASA for a supercomputer grant.

References and Notes

(1) Pacchioni, G. Cluster Modelling of Oxide Surfaces: Structure, Adsorption and Reactivity. In *Chemisorption and Reactivity on Supported Clusters and Thin Films: Towards an Understanding of Microscopic Processes in Catalysis*; Lambert, R. M., Pacchioni, G., Eds.; NATO ASI Series; Plenum: New York, 1997; Vol. 331.

(2) Schulte, F. K. *Surf. Sci.* **1976**, *56*, 427−444.

(3) Kolb, D. M.; Przasnyski, M.; Gerischer, H. *J. Electroanal. Chem.* **1974**, *54*, 25.

(4) Leiva, E.; Schmickler, W. *Chem. Phys. Lett.* **1989**, *160*, 75−79.

(5) Gerischer, H.; Kolb, D. M.; Przasnyski, M. *Surf. Sci.* **1974**, *43*, 282.

(6) Miura, K.; Yamada, A.; Tanaka, M. *Electrochim. Acta* **1996**, *41*, 249−256.

(7) Wandelt, K. *Appl. Surf. Sci.* **1997**, *111*, 1−10.

(8) Riviere, J. C. Work function: measurements and results. In *Solid State Science*; Green, M., Ed.; Marcel Dekker: New York, 1969; pp 179−289.

(9) Lang, N. D.; Kohn, W. *Phys. Rev. B* **1970**, *1*, 4555−4568.

(10) Lang, N. D.; Kohn, W. *Phys. Rev. B* **1971**, *3*, 1215−1223.

(11) Lang, N. D. *Phys. Rev. B* **1971**, *4*, 4234−4245.

(12) Lang, N. D.; Kohn, W. *Phys. Rev. B* **1973**, *7*, 3541−3550.

(13) Alonso, J. A.; March, N. H. *Electrons in metals and alloys*; Academic Press: London, 1989.

(14) Ashcroft, M. *Solid-state physics*; Sounders College Publishing: Orlando, FL, 1976.

(15) Haberlen, O. D.; Chung, S. C.; Stener, M.; Rosch, N. *J. Chem. Phys.* **1997**, *106*, 5189−5201.

(16) Kiejna, A.; Pogosov, V. V. *J. Phys.: Condens. Matter* **1996**, *8*, 4245−4257.

(17) Pacchioni, G.; Chung, S. C.; Kruger, S.; Rosch, N. *Chem. Phys.* **1994**, *184*, 125−137.

(18) Ross, R. B.; Ermler, W. C.; Kern, C. W.; Pitzer, R. M. *Int. J. Quantum Chem.* **1992**, *41*, 733−747.

(19) Li, Y. S.; Daelen, M. A. v.; King-Smith, D.; Wrinn, M.; Wimmer, E.; Newsam, J. M.; Klitsner, T.; Sears, M. P.; Carlson, G.; Nelson, J.; Allan, D. C.; Teter, M. P. Density functional methods and applications to materials problems. *Mater. Res. Soc. Symp. Proc.*, 1994.

(20) Seminario, J. M.; Tour, J. M. Ab initio methods for the study of molecular systems for nanometer technology. In *Molecular electronics: science and technology*; Aviram, A., Ratner, M., Eds.; Annals of the New York Academy of Sciences: New York, 1998.

(21) Tour, J. M.; Kozaki, M.; Seminario, J. M. *J. Am. Chem. Soc.* **1998**, *120*, 8486−8493.

(22) Seminario, J. M.; Zacarias, A. G.; Tour, J. M. *J. Am. Chem. Soc.* **1998**, *120*, 3970−3974.

(23) Seminario, J. M.; Tour, J. M. *Int. J. Quantum Chem.* **1997**, *65*, 749−758.

(24) Hoffmann, R. *Solids and Surfaces, a Chemist's View of Bonding in Extended Structures*; VCH Publishers: New York, 1988.

(25) *Modern Density Functional Theory: A Tool for Chemistry*; Seminario, J. M., Politzer, P., Eds.; Elsevier: Amsterdam, 1995.

(26) *Recent Developments and Applications of Modern Density Functional Theory*; Seminario, J. M., Ed.; Elsevier Science Publishers: Amsterdam, 1996; Vol. 4.

(27) *Recent Advances in Density Functional Theory (Part I)*; Chong, D. P., Ed.; World Scientific: Singapore, 1995.

(28) Parr, R. G.; Yang, W. *Density Functional Theory of Atoms and Molecules*; Oxford University Press: Oxford, 1989.

(29) Kryachko, E. S.; Ludeña, E. *Energy Density Functional Theory of Many-electron Systems*; Academic Press: New York, 1990.

(30) Dreizler, R. M.; Gross, E. K. U. *Density Functional Theory*; Springer-Verlag: Berlin, 1990.

(31) Labanowski, J. K.; Andzelm, J. W. *Density functional methods in chemistry*; Springer-Verlag: New York, 1991.

(32) Hay, P. J.; Wadt, W. R. *J. Chem. Phys.* **1985**, *82*, 270−283.

(33) Wadt, W. R.; Hay, P. J. *J. Chem. Phys.* **1985**, *82*, 284−298.

(34) Becke, A. D. *J. Chem. Phys.* **1993**, *98*, 5648−5652.

(35) Perdew, J. P. Unified theory of exchange and correlation beyond the local density approximation. In *Electronic Structure of Solids*; Ziesche, P., Eschrig, H., Eds.; Akademie Verlag: Berlin, 1991.

(36) Perdew, J. P.; Chevary, J. A.; Vosko, S. H.; Jackson, K. A.; Pederson, M. R.; Singh, D. J.; Fiolhais, C. *Phys. Rev. B* **1992**, *46*, 6671−6687.

(37) Perdew, J. P.; Wang, Y. *Phys. Rev. B* **1992**, *45*, 13244−13249.

(38) Frisch, M. J.; Trucks, G. W.; Schlegel, H. B.; Gill, P. M. W.; Johnson, B. G.; Robb, M. A.; Cheeseman, J. R.; Keith, T.; Petersson, G. A.; Montgomery, J. A.; Raghavachari, K.; Al-Laham, M. A.; Zakrzewski, V. G.; Ortiz, J. V.; Foresman, J. B.; Peng, C. Y.; Ayala, P. Y.; Chen, W.; Wong, M. W.; Andres, J. L.; Replogle, E. S.; Gomperts, R.; Martin, R. L.; Fox, D. J.; Binkley, J. S.; Defrees, D. J.; Baker, J.; Stewart, J. P.; Head-

Gordon, M.; Gonzalez, C.; Pople, J. A. *GAUSSIAN 94*, revision E.1; Gaussian Inc.: Pittsburgh, 1997.

(39) Peng, C.; Ayala, P. Y.; Schlegel, H. B.; Frisch, M. J. *J. Comput. Chem.* **1996**, *17*, 49−56.

(40) Neyman, K. M.; Pacchioni, G.; Rosch, N. Adsorption complexes on oxides: density functional model cluster studies. In *Recent developments and applications of modern density functional theory*; Seminario, J. M., Ed.; Elsevier: Amsterdam, 1996; pp 569−619.

(41) Hoffmann, R.; Lipscomb, W. N. *J. Chem. Phys.* **1962**, *36*, 3489.

(42) Baetzold, R. C. *J. Phys. Chem.* **1978**, *82*, 738−744.

(43) Leopold, D. G.; Ho, J.; Lineberger, W. C. *J. Chem. Phys.* **1987**, *86*, 1715.

(44) Jackson, K. A. *Phys. Rev. B* **1993**, *47*, 9715−9722.

(45) Richtsmeier, S. C.; Dixon, D. A.; Gole, J. L. *J. Phys. Chem.* **1982**, *86*, 3937−3941.

(46) Howard, J. A.; Preston, K. F.; Sutcliffe, R.; Mile, B. *J. Phys. Chem.* **1983**, *87*, 536−537.

(47) Mulliken, R. S. *J. Chem. Phys.* **1955**, *23*, 1833, 1841, 2338, 2343.

(48) Politzer, P.; Truhlar, D. G. *Chemical Applications of Atomic and Molecular Electrostatic Potentials*; Plenum Press: New York, 1981.

(49) Burdett, J. K. *Chemical bonding in solids*; Oxford: New York, 1995.

(50) Kittel, C. *Introduction to solid-state physics*, 4th ed.; Wiley: New York, 1971.

(51) Wachters, A. J. H. *J. Chem. Phys.* **1970**, *52*, 1033−1036.

(52) Huber, K. P.; Herzberg, G. *Molecular spectra and molecular structure*; Van Nostrand-Reinhold Company: Ottawa, 1978.

(53) Payami, M.; Nafari, N. *J. Chem. Phys.* **1998**, *109*, 5730−5740.

(54) Knickelbein, M. *Chem. Phys. Lett.* **1992**, *192*, 129.

(55) Zhao, J. J.; Han, M.; Wang, G. H. *Phys. Rev. B* **1993**, *48*, 15297−15300.

(56) Zhao, J.; Chen, X.; Wang, G. *Chem. Phys. Lett.* **1996**, *254*, 21−24.

(57) *Handbook of Chemistry and Physics*, 77th ed.; Lide, D. R., Ed.; CRC Press: Boca Raton, 1997.

(58) Perdew, J. P.; Parr, R. G.; Levy, M.; Balduz, J. L., Jr. *Phys. Rev. Lett.* **1982**, *49*, 1691−1694.